Glasnik hemičara i tehnologa Bosne i Hercegovine

Bulletin of the Chemists and Technologists of Bosnia and Herzegovina

2025

65

Proceedings

Print ISSN: 0367-4444

Online ISSN: 2232-7266

DOI: 10.35666/2232-7266.2025.65.04

UDK:544.08[546.62:621.564.3]

35-44

Electrochemical Behaviour of Aluminum in Artificial Seawater in the Presence of *Artemisia annua* L.

Zlatić Jelić G., Pilić, Z.*, Martinović, I., Čelan, S., Pejak, L.

Faculty of Science and Education, University of Mostar, Bosnia and Herzegovina

Article info
Received: 09/09/2024
Accepted: 28/08/2025

Keywords:
Plant Extracts
Green Inhibitors
Aluminum
Corrosion
Seawater
Electrochemical methods

***Corresponding author:**
Zora Pilić
E-mail: zora.pilic@fpmoz.sum.ba
Phone: +387 36 445 464

Abstract: This study investigated the use of *Artemisia annua* L. aqueous extract as a corrosion inhibitor for aluminum in artificial seawater using cyclic voltammetry (CV), potentiodynamic polarization (PP) and electrochemical impedance spectroscopy (EIS) measurements. The surface film formed on the Al in the presence of *A. annua* was analyzed using Fourier-transform infrared (FTIR) spectroscopy. Electrochemical results showed that *A. annua* is a mixed type inhibitor of Al corrosion with predominantly anodic action and is changing the electrochemical behavior of Al in artificial seawater by inhibiting dissolution processes. The inhibition efficiency of ~91% was attributed to the formation of a homogenous multilayer composed of phenolic acids. According to the results of FTIR analysis, the adsorption was established through the carboxyl group of phenolic acids, where stabilization of the adsorption layer was achieved through interactions between aromatic rings and the aliphatic chains. The adsorption mechanism obeyed the Freundlich isotherm model and El-Awady kinetic-thermodynamic models and referred to physical adsorption (ΔG_{ads} = 18.83 ± 2.34 kJ mol^{-1}).

INTRODUCTION

Aluminum is a widely used metal in the production of marine structures and the shipbuilding industry for its resistance to corrosion and low density, which improves performance and reduces the fuel consumption of ships (Ashkenazi, 2019). The resistance to corrosion results from the formation of a thin, stable oxide layer on the surface, which acts as a protective barrier against further oxidation of the aluminum and thereby reduces the rate of corrosion processes (Ashkenazi, 2019, Vargel, 2020). However, in the presence of chlorides that can specifically adsorb on the charged metal surface and penetrate the surface film Melchers, 2014), localized change in the potential can occur resulting in localized corrosion known as pitting. From ecological and economic aspects, localized corrosion is a significant threat to various industries as it can lead to structural damage, injuries, and the potential release of harmful substances into the environment (Jia, Unsal, Xu et al, 2019). This raises another concern associated with the protective measures against corrosion since any materials contributing to the pollution of the marine environment complicate the application of chemical substances, including those used in marine coatings and corrosion inhibitors.

European Union Water Framework Directive (2000/60/EC) emphasizes the need to reduce pollution from hazardous substances, which can include certain chemicals used in coatings and corrosion inhibitors (http-1). For example, tributyltin (TBT), once commonly used in antifouling paints, has been banned due to its toxic effects on marine organisms (Amara, Miler, Ben Slama et al, 2018). The shift toward sustainable practices includes the use of non-toxic corrosion protection methods, such as the use of natural inhibitors that do not leach harmful substances into the environment (Jia, Unsal, Xu et al, 2019; Zlatić, Martinović. Pilić et al, 2023). Plants are the richest source of natural antioxidants with polyphenolics being the most prevalent (Pratt, 1992, Kaur, Daksh, Saxena, 2024). These compounds can be found throughout all parts of the plant and can offer a base for the development of renewable natural inhibitors of corrosion processes (Kaur, Daksh, Saxena, 2024). In our earlier studies, the aqueous extraction of *Artemisia annua* L. was carried out at room temperature, intentionally avoiding the use of excessive energy and solvents that typically produce a significant amount of waste by-products in plant extract preparation (Zlatić, Martinović. Pilić et al, 2023; Zlatić, Martinović. Pilić et al, 2024). The extract showed 80% inhibition efficiency toward corrosion of aluminum alloy in both abiotic (Zlatić, Martinović. Pilić et al, 2023) and biotic simulated marine environment (Zlatić, Martinović. Pilić et al, 2024) which was attributed to the physical adsorption of caffeic acid derivatives on the alloy surface, as well

formation of a protective Al_2O_3. *A. annua* grows naturally on the North hemisphere in moderate climates and poses extraordinary antibacterial, antioxidant and antiviral properties (Zlatić, Martinović. Pilić et al, 2024, Zlatić, Martinović. Pilić et al, 2023b) wherefore can replace hazardous chemicals used in protection measures against corrosion. Taking into account the wide application of aluminum and that protecting existing constructions can reduce waste and promote sustainability, an investigation of the influence of *A. annua* on aluminum corrosion can contribute to the development of effective, environmentally friendly protective measures against corrosion. So the purpose of the investigations was twofold; (1) characterization of the electrochemical properties of aluminum in the artificial seawater without and with the addition of *A. annua* extract and (2) characterization of the adsorption layer using empirical models and Fourier transform infrared (FTIR) spectroscopy.

EXPERIMENTAL

The electrochemical measurements were executed in a standard three electrode cell using an Autolab PGSTAT320N potentiostat that was controlled by Nova 1.5 software. Electrochemical cell was composed of aluminum (99.99%) as a working electrode, platinum sheet as a counter electrode and the Ag | AgCl | 3 M KCl reference electrode. The working electrolyte was artificial seawater with the following chemical composition (g/L): 4.1575 Na_2SO_4, 11.1211 $MgCl_2x6H_2O$, 0.79023 KCl, 1.5877 $CaCl_2x2H_2O$, 24.9772 NaCl, 0.0587 $NaHCO_3$ (Zlatić, Martinović. Pilić et al, 2023a, Zlatić, Martinović. Pilić et al, 2024, Zlatić, Martinović. Pilić et al, 2023b, Dickson, 1990). The *A. annua* aqueous extract was prepared according to the procedure described previously (Zlatić, Martinović. Pilić et al, 2023a, Zlatić, Martinović. Pilić et al, 2024, Zlatić, Martinović. Pilić et al, 2023b), using the same batch of plant material. The phytochemical profile of *A. annua* extract, including HPLC (Zlatić, Martinović. Pilić et al, 2023a) and FTIR (Zlatić, Martinović. Pilić et al, 2024) analyses, is available in previously published studies. Briefly, 1.0 g of dried plant was mixed with 1.0 L of working electrolyte and set aside in dark for 3h. The sample was then filtered using 0.45 μm filter paper and diluted up to 1.0 L. Prior each measurement aluminum was abraded by SiC emery paper (360-1000 grades), degreased in ethanol using an ultrasonic bath and polarized at –1.60 V for 2 minutes.

The electrochemical properties of aluminum without and with the addition of *A. annua* were studied using cyclic voltammetry (CV), electrochemical impedance spectroscopy (EIS), and potentiodynamic polarization (PP) measurements. Cyclic voltamograms were taken in the potential range from –1.60 to –0.70 V with the scan rate of 30 mVs^{-1}. EIS was carried out at the open circuit potential (EOCP) that was measured until the stationary state was attained which was approximately 60 minutes. The spectra were taken in the frequency range from 10 kHz to 5 mHz using alternating voltage of 10 mV. Right after EIS measurements, PP curves were obtained at a scan rate of 1 mVs^{-1} in the potential range of ± 0.20 V vs. EOCP.

The presence of functional groups of *A. annua* extract on the Al surface was investigated using a Fourier transform infrared (FTIR) spectrometer IRAffinity-1S (Shimadzu, Japan) coupled with single reflection type attenuated total reflection (ATR) attachment (GladiATR10, Shimadzu, Japan). For this purpose, working electrodes were immersed in working electrolyte with and without the addition of 1 gL^{-1} *A. annua* extract for 24h, after which the electrode surfaces were dehydrated with the series of ethanol solutions (v/v: 50%, 75%, and 96%). FTIR spectrum was taken directly from the surfaces in the wavelength range between 400 and 4000 cm^{-1}.

RESULTS AND DISCUSSION

Cyclic voltammetry

Cyclic voltammograms of aluminum recorded in artificial seawater with and without the addition of *A. annua* are shown in Figure 1. It can be seen that the cyclic voltammogram recorded without *A. annua* show current shoulder at around −1.3 V associated with the accumulation of cations and anions on the Al surface (Hasenay and Šeruga, 2007). Anodic current densities around this potential decreased with the increasing concentration of *A. annua*. Another anodic peak was observed around −0.8 V, but only in the cyclic voltammogram recorded with the addition of 0.5 g L^{-1} *A. annua*, and corresponds to the formation of Al_2O_3 (Zlatić, Martinović. Pilić et al, 2023a, Hasenay and Šeruga, 2007). A decrease in the diffusion rate of aluminium ions from the electrode surface on the electrode/electrolyte interface, and the formation of an oxide film with protective properties are typical features of anodic inhibitors that decrease anodic active sites of metal (Martinović, Zlatić, Pilić et al., 2023). A decrease in the active area of the metal is achieved either by the adsorption of inhibitor molecules onto the charged metal surface or by promoting the formation of protective films (Salci, Yukel and Solmaz, 2022). From the presented cyclic voltammograms (Figure 1) the total amount of anodic charge, QA per unit of the Al surface was determined by integrating the area under the anodic current. The obtained values were then used in the calculation of the surface coverage Θ of the working electrode with the inhibitor using Equation 1 (Ma, Ammar, Kumar et al, 2022):

$$\Theta = \frac{Q_A - Q'_A}{Q_A} \qquad (1)$$

Here, QA and Q'A refer to anodic charges determined from cyclic voltammograms of aluminum in artificial seawater without and with the addition of *A. annua*, respectively. As the amount of adsorbed inhibitor on the alloy surface is quantitatively related to the inhibition efficiency, *A. annua* inhibition efficiency (IE) toward Al corrosion in artificial seawater was calculated with the following equation:

$$IE = \Theta \cdot 100 \qquad (2)$$

Table 1 shows results of CV analysis. The amount of anodic charges (QA) decreased with the increasing concentration of *A. annua*. When 1 gL^{-1} of *A. annua* was added to the artificial seawater, almost the entire aluminium surface was covered with inhibitor resulting in a maximum IE of 99%.

Table 1. The values of the parameters obtained by analyzing the experimental results from Figure 1.

γ (g L^{-1})	Q_A (µC cm^{-2})	θ	*IE* (%)
0	71	-	-
0.10	65	0.084	8.42
0.25	55	0227	22.77
0.50	11	0.838	83.83
1.00	0.013	0.999	99.98

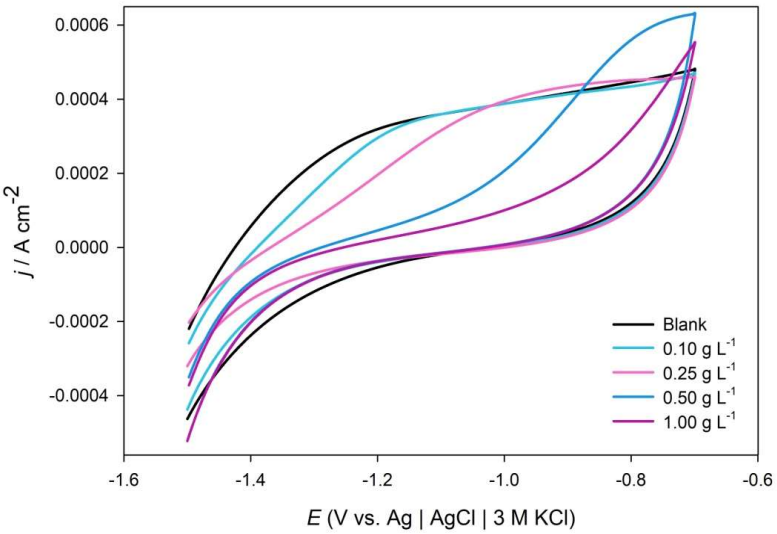

Figure 1. Cyclic voltammograms recorded on aluminum in artificial seawater at a scan rate of 30 mV/s, without and with the addition of different concentrations of *A. annua* (marked in the figure).

Potentiodynamic Polarization

Figure 2 shows potentiodynamic polarization (PP) curves recorded in artificial seawater without and with the addition of different concentrations of *A. annua*. Analyzing the PP curves provided insight into the corrosion kinetic parameters such as the Tafel slopes (bA, bC), corrosion potentials (Ecorr), and corrosion current densities (jcor). These values are useful for assessing the influence of inhibitors on the electrochemical behavior of metals, allowing the calculation of the working electrode's surface coverage Θ by the inhibitor using the corrosion current densities (eq. 3) Martinović, Zlatić, Pilić et al., 2023).

$$\Theta = \frac{j_{cor}^{0} - j_{cor}}{j_{cor}^{0}} \qquad (3)$$

Where j_{cor}^{0} and j_{cor} are corrosion current densities deduced from PP curves recorded without and with the addition of *A. annua*. The values of kinetic parameters obtained by analyzing the results from Figure 2 are given in Table 2 along with the inhibition efficiencies and surface coverage calculated using Equations 2 and 3.

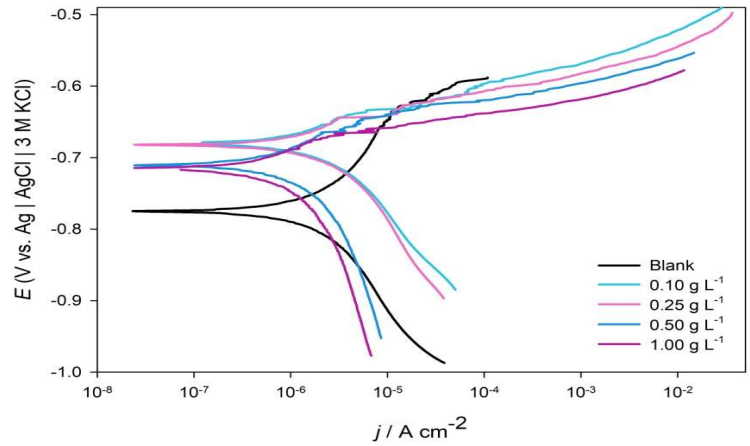

Figure 2. Potentiodynamic polarization curves recorded on aluminum in artificial seawater at a scan rate of 1 mV s^{-1}, without and with the addition of different concentrations of *A. annua* (marked in the figure)

Table 2. The values of the corrosion parameters obtained by analyzing the experimental results from Figure 2.

γ (g L^{-1})	b_a (V dec^{-1})	b_c (V dec^{-1})	E_{corr} (V)	j_{corr} (μA cm^{-2})	θ	IE (%)
0	0.052	0.052	−0.775	0.567		
0.1	0.032	0.029	−0.681	0.405	0.285	28.5
0.25	0.028	0.024	−0.683	0.360	0.365	36.5
0.50	0.035	0.038	−0.710	0.242	0.572	57.2
1.00	0.024	0.023	−0.716	0.130	0.771	77.1

As can be seen from Figure 2, adding *A. annua* to artificial seawater resulted in a positive shift in the corrosion potential of aluminum. The anodic reaction rate with the addition of *A. annua* was controlled by charge transfer, as recognized by an increase in the reaction rate with increasing potential (Fig. 2). Also, both anodic and cathodic Tafel slopes slightly decreased after the plant extract was added to the artificial seawater, indicating that *A. annua* acts as a mixed type corrosion inhibitor for Al (Salci, Yukel and Solmaz, 2022), with a predominant anodic action recognized by a positive shift of corrosion potential after the addition of *A. annua* to the artificial seawater (Zlatić, Martinović. Pilić et al, 2023a, Martinović, Zlatić, Pilić et al., 2023). An increase in the concentration of the inhibitor resulted in a decrease in jcor. Withal, the inhibition efficiency of *A. annua* toward Al corrosion in artificial seawater increased with the increasing concentration of the extract, reaching a maximum of 77% at 1 gL^{-1} (Table 2).

Electrochemical Impedance Spectroscopy

Impedance spectra of Al electrodes recorded at open circuit potential in artificial seawater without and with the addition of extract in different concentrations are presented by Nyquist and Bode plots in Figure 3. The obtained data showed the capacitive behavior of the electrode in the middle-frequency range for all examined conditions. Simultaneously, an inductive loop was observed on the Nyquist plot in the low-frequency region for aluminum immersed in artificial seawater and in the presence of 0.10 g L^{-1} of the extract. This feature, also visible in Bode plots as a positive phase shift at low frequencies, has been previously linked to the dynamic dissolution of the surface oxide film and the participation of adsorbed intermediates in the electrochemical process (Yang, Yuan, Liu et al, 2017, Ma, Lis Chen et al, 2002). According to the model proposed by H. Ma et al. (Ma, Lis Chen et al, 2002), the occurrence of inductive behavior can arise in systems involving sequential reaction steps with adsorbed intermediates. Specifically, the inductive loop appears when the rate-determining step shifts between adsorption and desorption of the intermediate, i.e., when the ratio of adsorption/desorption rate constants changes as a function of electrode potential.

The disappearance of the inductive loop at higher concentrations of *A. annua* extract (≥ 0.25 g L^{-1}) suggested a shift in surface reaction dynamics, likely caused by the formation of a more stable organic layer that suppressed the formation or participation of such intermediates. This is in line with the "chemical inductor" framework described by J. Bisquert and A. Guerrero (2022), where inductive elements in electrochemical systems arise from coupling between fast charge transfer processes and slower surface phenomena such as intermediate formation, surface restructuring, or inhibitor reorganization. As seen from Figure 3, the radius of the capacitive semicircle increased with increasing the inhibitor's concentration. These observations indicate that the adsorbed organic molecules at higher extract concentrations inhibit the dynamic processes responsible for inductive behavior, resulting in a more ideal capacitive response. This supports the interpretation that *A. annua* acts as a surface-blocking inhibitor, stabilizing the electrode interface and shifting the mechanism away from dynamic dissolution toward surface passivation. The results of EIS measurements were interpreted using electrical equivalent circuits (EEC) presented in Figure 4. Values of EEC elements are given in Table 3.

EEC presented in Figure 4a was assigned to EIS results recorded in artificial seawater without and with the addition of 0.10 g L^{-1} *A. annua*. The electrochemical behavior of Al during the addition of higher concentrations of *A. annua* (0.25-1.00 gL^{-1}) was described with a simplified Randless cell (Figure 4b). In these EECs, R represents the ohmic resistance of the working electrolyte, R1 and Q1 charge transfer resistance, and constant phase element (CPE) associated with the double-layer capacitance. R2 and L refer to resistance and inductance of the modified surface layer (Yang, Yuan, Liu et al, 2017, Ma, Lis Chen et al, 2002, Bisquert and Guerrero, 2022). Compared with bare electrolyte, charge transfer resistance R1 in the presence of *A. annua* (0.25-1.00 g L^{-1}) notably increased. Meanwhile, the CPE associated with the capacitance of the electrical double-layer decreased (Table 3). This was due to a decrease in local dielectric constants of the surface layer and/or the formation of a thicker electrical double-layer as a consequence of the adsorption of inhibitors on the electrode surface that protected aluminum from further corrosion (Martinović, Zlatić, Pilić et al., 2023). The addition of *A. annua* to artificial seawater also decreased surface heterogeneity as recognized by an increase in n values (Table 3). For the evaluation of the surface coverage Θ by extract, the total resistance to polarization Rp was taken into account and calculated according to Equation 4 (Zlatić, Martinović. Pilić et al, 2023b, Chellouli, Chebabe, Dermai et al, 2016):

$$\Theta = \frac{R'_P - R_P}{R'_P} \qquad (4)$$

Here, R_P and 〚R'〛_P are the polarization resistances recorded without and with the addition of *A. annua*. RP represented a sum of R1 and R2 for the results described

with two-time constants whereas for a one-time constant model RP = R1 (Zlatić, Martinović. Pilić et al, 2023b, Chellouli, Chebabe, Dermai et al, 2016) Surface coverage deduced from EIS data was also used in determining the inhibition efficiency (IE) of the extract using Equation 2. As presented in Table 3, IE increased with an increase in *A. annua* concentration ranging from 29-97%.

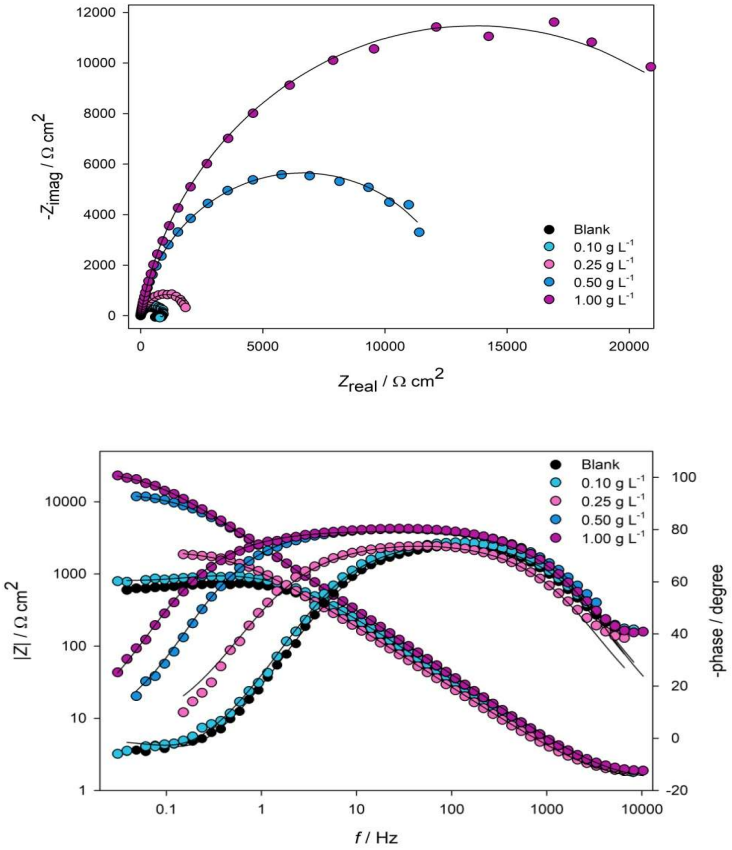

Figure 3. Nyquist and Bode plots of impedance spectra recorded on aluminum in artificial seawater without and with the addition of different concentrations of *A. annua* (marked in the figure).

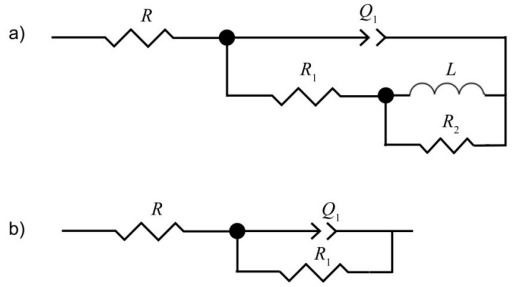

Figure 4. Equivalent electrical circuits used in modeling the impedance spectra presented in Figure 3, where Q_1 represents the constant phase element (*CPE*) associated with the capacitance of the electrical double layer.

Table 3. Values of the EECs for aluminum in artificial seawater without and with the addition of *A. annua*, obtained by analyzing the experimental results from Figure 3.

γ	*R*	*CPE* x 10^4	n_1	R_1	R_2	*L*	θ	*IE*
g L^{-1}	Ω cm^2	$Ω^{-1}s^n$ cm^{-2}		Ω cm^2	Ω cm^2	H cm^2		%
0	1.2	1.21	0.857	629.6	103.40	132.3		
0.10	1.2	1.12	0.986	803.1	235.90	131.6	0.29	29.4
0.25	1.3	1.58	0.848	1765.8	-	-	0.58	58.5
0.50	1.2	0.77	0.901	11229.0	-	-	0.93	93.5
1.00	1.3	0.81	0.898	21005.0	-	-	0.96	96.5

A comparison with our previous study (Zlatić, Martinović. Pilić et al, 2023a) highlights both consistencies and novel observations. In both works, the addition of *A. annua* extract led to an increase in polarization resistance and a decrease in double-layer capacitance, consistent with the formation of a protective surface layer. However, in the present study, electrochemical impedance spectra recorded at lower extract concentrations (0.10 gL^{-1}) revealed a low-frequency inductive loop (Fig. 3), which was not observed in our previous work (Zlatić, Martinović. Pilić et al, 2023a). Consequently, equivalent circuit modelling in this study required two-time constant elements at low extract concentration, whereas in earlier study a single-time constant (Randles-type) circuit applied for all conditions. This distinction suggests that the lower concentrations of the extract in this study allow for transient processes at the electrode interface, such as the formation and desorption of adsorbed intermediates, which contribute to the observed inductive behavior (Ma, Lis Chen et al, 2002, Bisquert and Guerrero, 2022). At higher extract concentrations, these processes are likely suppressed due to more complete surface coverage, resulting in a capacitive response similar to that observed in our earlier work (Zlatić, Martinović. Pilić et al, 2023a).

Adsorption mechanism

All electrochemical results showed an increase in the inhibition efficiency of *A. annua* against aluminum corrosion in artificial seawater with increasing extract concentration. The latter was associated with the adsorption of *A. annua* extract on the aluminum surface, so the surface coverage (Θ) calculated using Equations 1, 2, and 4 were utilized in the assessment of the adsorption mechanism. Therefore, different adsorption isotherms were tested to get insight into interactions between extract molecules and aluminum surface. The best fitting isotherm model that reflects the adsorption process of *A. annua* on Al surface in artificial seawater was the Freundlich adsorption isotherm (Figure 5) that can be expressed with the Equation 5 (Khamis, Bellucci, Latanision et al, 1991, Al-Ghouti and Da'ana, 2020):

$$\log \Theta = \log K_{\text{ads}} - \frac{1}{n}\log \gamma \quad (5)$$

Here, Θ is the surface coverage; γ is the concentration of extract in g L^{-1}, while parameters K_ads and 1/n indicate constant and the intensity of adsorption and are dependent on the temperature. 1/n determines the intensity of adsorption, that is, surface heterogeneity, which indicates the relative energy distribution and heterogeneity of adsorbate sites (Al-Ghouti and Da'ana, 2020). The Freundlich isotherm model describes a heterogeneous surface assuming that adsorption processes occur in a multilayer way and that each inhibitor molecule has a different adsorption potential (Ituen, Akaranta and James, 2017). The formation of a multilayer can also be discussed in terms of the El-Awady kinetic-thermodynamic model (El-Awady, Abd-El-Nabey, Azis, 1992, ,Martinović, Pilić, Zlatić et al, 2023, Thabet, EL-Moselhy, Azooz et al, 2024):

$$\log\left(\frac{\theta}{1-\theta}\right) = \log K + a\log \gamma \quad (6)$$

Here K is the constant, and 1/a is the number of the active sites occupied by one inhibitor molecule. If the multilayer of the inhibitor was formed on the metal surface, a value of 1/a is less than 1. If it's above 1, the inhibitor occupies more than one active site ,(Martinović, Pilić, Zlatić et al, 2023). From parameters obtained by the El-Awady kinetic model (Figure 6), the value of the adsorption constant, Kads can be calculated using the following equation (El-Awady, Abd-El-Nabey, Azis, 1992,(Martinović, Pilić, Zlatić et al, 2023, Thabet, EL-Moselhy, Azooz et al, 2024):

$$K_{ads} = K^{1/a} \quad (7)$$

The adsorption mechanism is determined by the free energy of adsorption ΔGads that can be calculated using corresponding Kads and the following equation:

$$\Delta G_{\text{ads}} = -RT\ln(K_{\text{ads}} c_{\text{w}}) \quad (8)$$

Where R is the universal molar gas constant (8.314 J K^{-1} mol^{-1}), T the temperature (298K) and cw is the mass concentration of water in the working electrolyte (1000 g L^{-1}) (Zlatić, Martinović. Pilić et al, 2023a, (Zlatić, Martinović. Pilić et al, 2023b, Chellouli, Chebabe, Dermai et al, 2016, (Martinović, Pilić, Zlatić et al, 2023). Values of Kads and ΔGads obtained from all applied models are presented in Table 4.

Table 4. Values of the parameters obtained by analyzing the experimental results from Figures 5 and 6.

Model	Method	R^2	$1/n$	$1/a$	K_{ads} (L g^{-1})	- ΔG (kJ mol^{-1})
Freudnlich isotherm	CV	0.945	1.152		1.26	17.69
	PP	0.973	0.447		0.75	16.43
	EIS	0.916	0.539		1.13	17.43
El-Awady	CV	0.838		0.409	3.28	20.07
	PP	0.936		1.06	3.01	19.85
	EIS	0.955		0.513	5.99	21.56

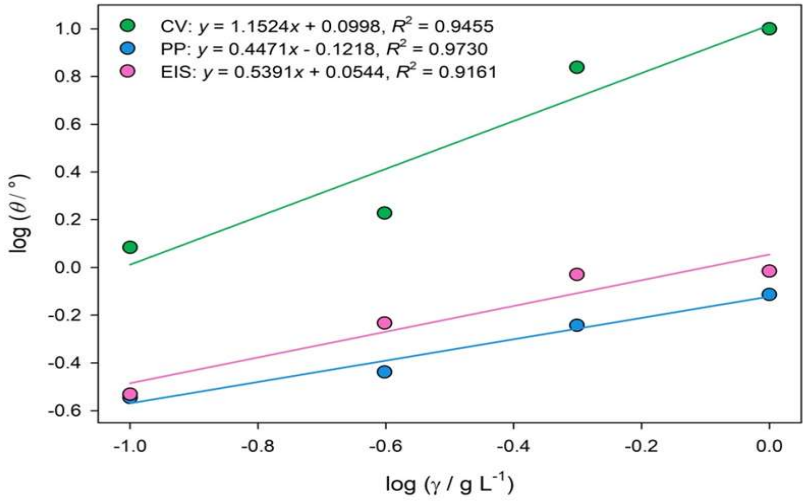

Figure 5. Freundlich adsorption isotherm of the adsorption of *A. annua* on the surface of an aluminum electrode in artificial seawater.

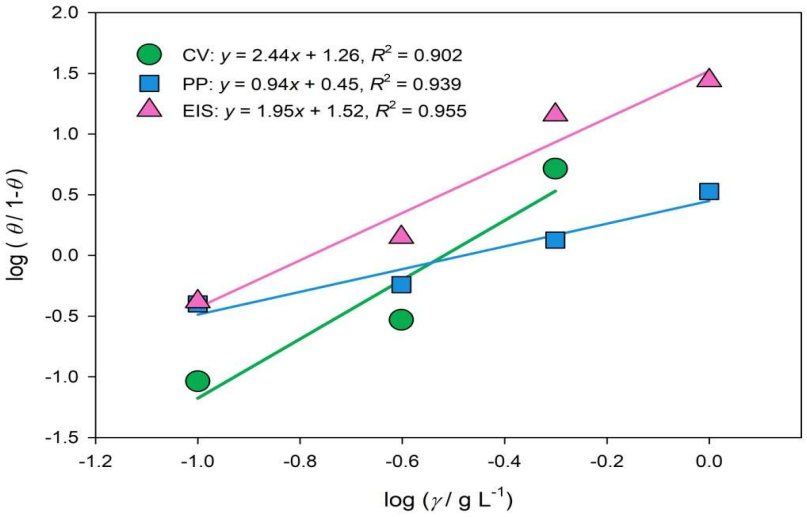

Figure 6. El-Awady kinetic–thermodynamic model of *A. annua* adsorption on the Al surface in artificial seawater

When describing the adsorption mechanism of the *A. annua* extract on the aluminum surface, the validity of selected thermodynamic models was proven by the achieved linearity (Figures 4 and 5) and further supported by the R2 values. As seen in Table 4, values of 1/a are equal to or less than 1, indicating that the inhibitor formed a multilayer on the Al surface (Martinović, Pilić, Zlatić et al, 2023). This is consistent with the assumptions proposed by the Freundlich isotherm model. The surface of the aluminum is assumed to have sites with different adsorption energies (Al-Ghouti and Da'ana, 2020). This heterogeneity can be due to the presence of oxides, defects, and other surface irregularities. Because the isotherm does not assume uniform free energy of adsorption, it is well-suited to describe systems where the free energy of adsorption decreases as the surface coverage increases, meaning high-energy sites are occupied first, and as more sites are filled, the remaining available sites have lower binding energies (Ituen, Akaranta and James, 2017).

From the values of the free energy of adsorption ΔGads calculated using Kads obtained from Freundlich isotherm model (−17.18 ± 0.66 kJ mol^{-1}, Table 4), as well as El-Awady model (−20.49 ± 0.93 kJ mol^{-1}, Table 4), it can be concluded that the inhibitor molecules are bounded to the charged Al surface by van der Waals forces, and the process corresponds to physical adsorption (Zlatić, Martinović. Pilić et al, 2023a, (Zlatić, Martinović. Pilić et al, 2023b, Chellouli, Chebabe, Dermai et al, 2016, El-Awady, Abd-El-Nabey, Azis, 1992, Martinović, Pilić, Zlatić et al, 2023) .

Fourier transform infrared spectroscopy

The FTIR spectra of the Al surface recorded after immersion in artificial seawater with and without the addition of 1 g L^{-1} *A. annua* extract are presented in Figure 7.

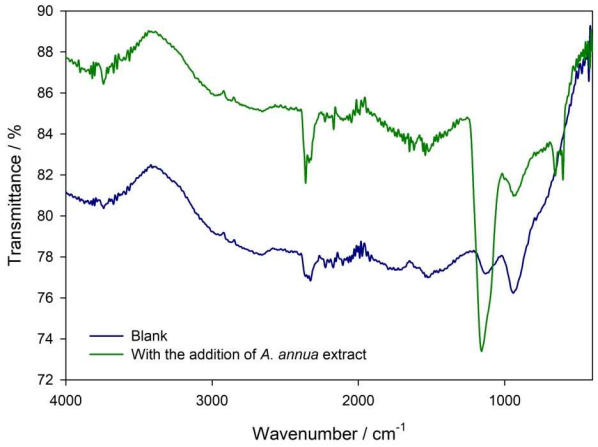

Figure 7. FTIR spectrum of the Al surface after immersion in the artificial seawater without and with the addition of 1 g L^{-1} *A. annua* extract.

A broad absorption band between 3800 and 3200 cm^{-1} was observed in both samples, corresponding to O–H stretching vibrations of adsorbed water and/or Al–OH surface groups. A band at approximately 1100 cm^{-1} was also present, and was attributed to surface Al–O (Zlatić, Martinović. Pilić et al, 2023a, (Zlatić, Martinović. Pilić et al, 2023b).

In contrast to the blank sample, the spectrum of the treated aluminum surface revealed several distinct peaks that were attributed to organic species adsorbed from the extract. A broad band in the range 3300–2500 cm^{-1} corresponding to the O–H stretching vibrations, likely originated from –OH groups present in caffeic and chlorogenic acid, as confirmed by our previous HPLC (Zlatić, Martinović. Pilić et al, 2023a, and FTIR (Zlatić, Martinović. Pilić et al, 2023b) analyses. A distinct band at approximately 1100 cm^{-1} was significantly more intense in the treated sample compared to the blank and was attributed to C–O stretching vibrations (Zlatić, Martinović. Pilić et al, 2023b, Iglesias, Garciade-Saldana, Jaen, 2001), confirming the presence of adsorbed organic molecules. Furthermore, two sharp bands appeared at approximately 655 cm^{-1} and 600 cm^{-1}, which were absent in the blank sample and were not observed in the FTIR spectrum of the extract itself (Zlatić, Martinović. Pilić et al, 2023b). These bands are characteristic of out-of-plane bending vibrations of aromatic C–H groups (Iglesias, Garciade-Saldana, Jaen, 2001), and their emergence only after exposure to the treated solution suggested surface-associated organization of adsorbed aromatic systems. The absence of a well-defined carbonyl stretching band around 1700 cm^{-1}, despite its presence in the extract (Zlatić, Martinović. Pilić et al, 2023b), suggested that the adsorption of phenolic acids occurred primarily via van der Waals forces, or π–π interactions rather than through coordination via carboxylate groups. This observation aligns with electrochemical data and calculated Gibbs adsorption energies (ΔGads = 18.83 ± 2.34 kJ mol^{-1}, Table 4), which point towards physisorption as the predominant interaction mechanism (Zlatić, Martinović. Pilić et al, 2023a, Chellouli, Chebabe, Dermai et al, 2016, El-Awady, Abd-El-Nabey, Azis, 1992, (Martinović, Pilić, Zlatić et al, 2023).

CONCLUSION

Plant extracts are affordable and eco-friendly corrosion inhibitors that could help transition to more sustainable protection measures of metals and alloys against corrosion failures. This work focused on the study of the electrochemical properties of Al in artificial seawater in the presence of *A. annua* using CV, PP, and EIS techniques. The surface of aluminum after treatment with *A. annua* was examined using ATR-FTIR spectroscopy. Electrochemical results showed that the addition of *A. annua* (0.25-1.00 g L^{-1}) to artificial seawater changed the electrochemical behavior of Al. This resulted in a decrease in corrosion current densities, as well as an increase in charge transfer resistance compared to bare electrolyte. According to corrosion kinetic parameters obtained from PP and CV measurements, *A. annua* extract acts as mixed type inhibitor of Al corrosion in artificial seawater with prevalent anodic action. Enhanced electrochemical properties were attributed to the adsorption of extract molecules onto the Al surface, as confirmed by the FTIR analysis. The adsorption mechanism was determined using the Freundlich adsorption isotherm and kinetic-thermodynamic model proposed by El-Awady et al. The estimated value of free energy of adsorption (ΔGads = 18.83 ± 2.34 kJ mol^{-1}) indicated physical adsorption of *A. annua* molecules on the charged Al surface. *A. annua* extract formed a multilayer and decreased the Al surface heterogeneity. This adsorbed layer played a role in modifying the electrochemical properties of the aluminum and enhancing its corrosion resistance.

ACKNOWLEDGEMENTS

The authors would like to acknowledge the financial support for the research from the Federal Ministry of Education and Science of Bosnia and Herzegovina.

REFERENCES

Al-Ghouti, M. A., & Da'ana, D. A. (2020). Guidelines for the use and interpretation of adsorption isotherm models: A review. *Journal of hazardous materials*, *393*, 122383. doi:10.1016/j.jhazmat.2020.122383

Amara, I., Miled, W., Slama, R. B., Ladhari, N. (2018). Antifouling processes and toxicity effects of antifouling paints on marine environment. A review. *Environmental toxicology and pharmacology*, *57*, 115-130.

Ashkenazi, D. (2019). How aluminum changed the world: A metallurgical revolution through technological and cultural perspectives. *Technological Forecasting and Social Change*, *143*, 101-113.

Bisquert, J., Guerrero, A. (2022). Chemical inductor. *Journal of the American Chemical Society*, *144*(13), 5996-6009.

Chellouli, M., Chebabe, D., Dermaj, A., Erramli, H., Bettach, N., Hajjaji, N., Casaletto M. P., Cirrincione, C., Privitera, A, Srhiri, A. (2016). Corrosion inhibition of iron in acidic solution by a green formulation derived from *Nigella sativa* L. *Electrochimica Acta*, *204*, 50-59.

Dickson, A. G. (1990). Thermodynamics of the dissociation of boric acid in synthetic seawater from 273.15 to 318.15 K. *Deep Sea Research Part A. Oceanographic Research Papers*, *37*(5), 755-766.

El-Awady, A. A., Abd-El-Nabey, B. A., Aziz, S. G. (1992). Kinetic-thermodynamic and adsorption isotherms analyses for the inhibition of the acid corrosion of steel by cyclic and open-chain amines. *Journal of the Electrochemical Society*, *139*(8), 2149.

Hasenay, D., Šeruga, M. (2007). The growth kinetics and properties of potentiodynamically formed thin oxide films on aluminium in citric acid solutions. *Journal of applied electrochemistry*, *37*(9), 1001-1008.

http-1 - https://www.eea.europa.eu/policy-documents/2008-56-ec (accessed 31st Aug 2024)

Iglesias, J., García de Saldaña, E., Jaén, J. A. (2001). On the tannic acid interaction with metallic iron. *Hyperfine Interactions*, *134*(1), 109-114.

Ituen, E., Akaranta, O., James, A. (2017). Evaluation of performance of corrosion inhibitors using adsorption isotherm models: an overview. Chemical science international journal, *18*(1), 1-34. https://doi.org/10.9734/csji/2017/28976

Jia, R., Unsal, T., Xu, D., Lekbach, Y., Gu, T. (2019). Microbiologically influenced corrosion and current mitigation strategies: A state of the art review. *International biodeterioration & biodegradation*, *137*, 42-58.

Kaur, J., Daksh, N., Saxena, A. (2022). Corrosion inhibition applications of natural and eco-friendly corrosion inhibitors on steel in the acidic environment: an overview. *Arabian Journal for Science and Engineering*, *47*(1), 57-74. https://doi.org/10.1007/s13369-021-05699-0

Khamis, E., Beliucci, F., Latanision, R. M., El-Ashry, E. S. H. (1991). Acid corrosion inhibition of nickel by 2-(triphenosphoranylidene) succinic anhydride. *Corrosion*, *47*(9), 677-686. doi:10.5006/1.3585307

Ma, H., Li, G., Chen, S., Zhao, S., Cheng, X. (2002). Impedance investigation of the anodic iron dissolution in perchloric acid solution. *Corrosion science*, *44*(6), 1177-1191.

Ma, I. W., Ammar, S., Kumar, S. S., Ramesh, K., Ramesh, S. (2022). A concise review on corrosion inhibitors: types, mechanisms and electrochemical evaluation studies. *Journal of Coatings Technology and Research*, *19*(1), 241-268. https://doi.org/10.1007/s11998-021-00547-0

Martinović, I., Pilić, Z., Zlatić, G., Soldo, V., Šego, M. (2023). *N*-Acetyl cysteine and D-penicillamine as green corrosion inhibitors for copper in 3% NaCl. *International journal of electrochemical science*, *18*(9), 100238. https://doi.org/10.1016/j.ijoes.2023.100238

Martinović, I., Zlatić, G., Pilić, Z., Šušak, M., Falak, F. (2023). Antioxidant capacity and corrosion inhibition efficiency of *Sambucus nigra* L. extract. *Chemical and biochemical engineering quarterly*, *37*(2), 79-87.

Melchers, R. E. (2014). Bi-modal trend in the long-term corrosion of aluminium alloys. *Corrosion Science*, *82*, 239-247. http://dx.doi.org/10.1016/j.corsci.2014.01.019

Nair, M. S., Huang, Y., Fidock, D. A., Polyak, S. J., Wagoner, J., Towler, M. J., Weathers, P. J. (2021). *Artemisia annua* L. extracts inhibit the in vitro replication of SARS-CoV-2 and two of its variants. *Journal of ethnopharmacology*, *274*, 114016. doi:10.1016/j.jep.2021.114016

Pratt, D. E. (1992). Natural antioxidants from plant material. American Chemical Society, In Phenolic Compounds in Food and Their Effects on Health II; Volume 507, pp. 54–71.

Salci, A., Yuksel, H., Solmaz, R. (2022). Experimental studies on the corrosion inhibition performance of 2-(2-aminophneyl) benzimidazole for mild steel protection in 1 M HCl solution. *Journal of the Taiwan institute of chemical engineers, 134*. https://doi.org/10.1016/j.jtice.2022.104349

Thabet, M., El-Moselhy, M. M., Azooz, R. E., El-Zomrawy, A. A. (2024). Rule of Lignosulfonate as a corrosion inhibitor for steel in neutral media, computational and reaction pathway. *Results in Surfaces and Interfaces*, *16*, 100266. https://doi.org/10.1016/j.rsurfi.2024.100266

Vargel, C. (2020). *Corrosion of aluminium*. Elsevier.

Yang, Q., Yuan, W., Liu, X., Zheng, Y., Cui, Z., Yang, X., Pan, H., Wu, S. (2017). Atomic layer deposited ZrO2 nanofilm on Mg-Sr alloy for enhanced corrosion resistance and biocompatibility. *Acta biomaterialia*, *58*, 515-526.

Zlatić, G., Martinović, I., Pilić, Z., Paut, A., Mitar, I., Prkić, A., Čulum, D. (2023). Green inhibition of corrosion of aluminium alloy 5083 by *Artemisia annua* L. extract in artificial seawater. *Molecules*, *28*(7), 2898. https://doi.org/10.3390/molecules28072898

Zlatić, G., Martinović, I., Pilić, Z., Kodranov, I., Ciganović, J., Sokol, V. (2023). The effect of *Artemisia annua* L. extract on microbiologically influenced corrosion of A36 steel caused by *Pseudomonas aeruginosa*. *Bioelectrochemistry*, *152*, 108447.

Zlatić, G., Martinović, I., Pilić, Z., Kovač, J., Čelan, S. (2024). Inhibition of microbiologically influenced corrosion of Al alloy 5083 in the presence of *Pseudomonas aeruginosa* by *Artemisia annua* L. *Journal of Electroanalytical Chemistry*, *975*, 118727. https://doi.org/10.1016/j.jelechem.2024.118727

Summary/Sažetak

Primjena vodenog ekstrakta *Artemisia annua* L. kao inhibitora korozije aluminija u umjetnoj morskoj vodi istražena je uz pomoć cikličke voltametrije (CV), potenciodinamičke polarizacije (PP) i elektrokemijske impedancijske spektroskopije (EIS). Površinski film formiran na Al u prisutnosti A. annua analiziran je korištenjem infracrvene spektroskopije s Fourierovom transformacijom (FTIR). Elektrokemijski rezultati pokazali su kako je *A. annua* mješoviti inhibitor Al korozije s pretežno anodnim djelovanjem koji mijenja elektrokemijsko ponašanje Al u umjetnoj morskoj vodi inhibicijom procesa otapanja aluminija. Učinkovitost inhibicije od ~91% pripisana je formiranju homogenog višesloja sastavljenog od fenolnih kiselina. Prema rezultatima FTIR analize, adsorpcija je uspostavljena preko karboksilne skupine fenolnih kiselina, gdje je stabilizacija adsorpcijskog sloja postignuta interakcijama između aromatskih prstenova i alifatskih lanaca. Mehanizam adsorpcije slijedio je Freundlichov model izoterme i El-Awadyjev kinetičko-termodinamički model te se odnosio na fizikalnu adsorpciju ($\Delta G_{ads} = 18.83 \pm 2.34$ kJ mol^{-1}).